Theor Appl Climatol (2011) 105:311–323
DOI 10.1007/s00704-010-0382-8

ORIGINAL PAPER

The influence of vegetation and building morphology on shadow patterns and mean radiant temperatures in urban areas: model development and evaluation

Fredrik Lindberg · C. S. B. Grimmond

Received: 30 August 2010 / Accepted: 9 December 2010 / Published online: 7 January 2011

Abstract The solar and longwave environmental irradiance geometry (SOLWEIG) model simulates spatial variations of 3-D radiation fluxes and mean radiant temperature (T_{mrt}) as well as shadow patterns in complex urban settings. In this paper, a new vegetation scheme is included in SOLWEIG and evaluated. The new shadow casting algorithm for complex vegetation structures makes it possible to obtain continuous images of shadow patterns and sky view factors taking both buildings and vegetation into account. For the calculation of 3-D radiation fluxes and T_{mrt}, SOLWEIG only requires a limited number of inputs, such as global shortwave radiation, air temperature, relative humidity, geographical information (latitude, longitude and elevation) and urban geometry represented by high-resolution ground and building digital elevation models (DEM). Trees and bushes are represented by separate DEMs. The model is evaluated using 5 days of integral radiation measurements at two sites within a square surrounded by low-rise buildings and vegetation in Göteborg, Sweden (57°N). There is good agreement between modelled and observed values of T_{mrt}, with an overall correspondence of R^2=0.91 (p<0.01, RMSE= 3.1 K). A small overestimation of T_{mrt} is found at locations shadowed by vegetation. Given this good performance a number of suggestions for future development are identified for applications which include for human comfort, building design, planning and evaluation of instrument exposure.

F. Lindberg · C. S. B. Grimmond
Environmental Monitoring and Modelling Group,
Department of Geography, King's College London,
Strand,
London WC2R 2LS, UK

F. Lindberg (✉)
Department of Earth Sciences, University of Gothenburg,
Box 460, Gothenburg SE-405 30, Sweden
e-mail: fredrikl@gvc.gu.se

1 Introduction

The increasing number of people living in urban areas accentuates the need for an improved understanding of how the environment within cities affects people's lives. The variation in urban microclimates produce a wide range of conditions which can impact people's health and well-being; for example, related to human thermal comfort. Predictions of human induced climate change suggest increases in surface air temperatures anywhere between 0.5 and 6.5°C over the next 100 years (IPCC 2007). In temperate climates, a 2–3°C increase in average summer temperatures will double the frequency of periods characterized by extremely high temperatures (WHO/WMO/UNEP 1996). This means that heat waves will become more frequent, more intense and last longer (Meehl and Tebaldi 2004). During extreme heat waves, as in central Europe in 2003, heat stress will have profound effects on people's health and well-being with substantial economic consequences (Pascal et al. 2006). By taking climate issues into consideration in the urban planning process by, for example, increasing the amount of vegetation in urban areas it may be possible to reduce the frequency of people suffering from heat stroke and increase overall comfort during heat waves in cities.

The long effect of vegetation on the urban climate has been investigated (e.g. Oke 1989; Honjo and Takakura 1990–1991; Akbari and Taha 1992; Akbari et al. 1997, 2001; Upmanis et al. 1998). Urban green structures reduce

air temperature by energy going in to evapotranspiration (latent heat flux) rather than sensible heat flux; shade parts of the ground and walls, which results in a reduction of the radiant temperature and impact wind velocity and direction; intercept the particulate matter that settles as temperatures decreases in the evening; and filter dust and noise. Considering the influence of vegetation on thermal comfort and the advocacy for it use (e.g. Greater London Authority 2010) in urban areas there are relatively few studies of its effect (e.g. Matzarakis et al. 1999; Picot 2004; Robitu et al. 2006; Ali-Toudert and Mayer 2007). These studies show foremost that vegetation shadowing can have a large effect in reducing heat stress in urban areas. However, typically these studies have been spatially constrained to one point or a small area such as a square or a street canyon.

Various thermal comfort indices have been developed to obtain an understanding of how humans interact with the outdoor climate (Fanger 1970; Gagge et al. 1986; Mayer and Höppe 1987). They work as tools to translate a combination of climatological data into one value which relates to the interaction between the human body and thermal conditions. As many were developed for indoor situations, a critical issue when moving outdoors is the change in radiation environment. This is considered in the mean radiant temperature (T_{mrt}) (Ali-Toudert et al. 2005) as it is the sum of all short- and longwave radiation fluxes (both direct and reflected) to which the human body is exposed. The T_{mrt} is defined as the 'uniform temperature of an imaginary enclosure in which radiant heat transfer from the human body equals the radiant heat transfer in the actual non-uniform enclosure' (ASHRAE 2001).

This paper explores the influence of vegetation and built morphology on mean radiant temperatures and shadow patterns in urban areas. Here the solar and longwave environmental irradiance geometry (SOLWEIG) model (Lindberg et al. 2008, hereafter referred to as L08) is used to investigate a large spatial domain.

2 Methods and materials

2.1 Model structure

Central to SOLWEIG is the calculation of T_{mrt}, which requires the six longwave and shortwave radiation fluxes (upward, downward and from the four cardinal points) to be determined from inputs of global shortwave radiation, air temperature and relative humidity (Höppe 1992). In order to determine T_{mrt} (units, K), the mean radiant flux density (R) is calculated, which is defined as the sum of all fields of long (L_i) and shortwave (K_i) radiation in three dimensions (i=1–6), together with the angular (F) and absorption (ξ_k) factors of an individual (VDI 1994, 1998):

$$R = \xi_k \sum_{i=1}^{6} K_i F_i + \varepsilon_p \sum_{i=1}^{6} L_i F_i \quad (1)$$

where F_i are the angular factors between a person and the surrounding surfaces. For a rotationally symmetric standing or walking person, F_i is set to 0.22 for radiation fluxes from the four cardinal points (east, west, north and south) and 0.06 for radiation fluxes from above and below (Fanger 1970). ξ_k is the absorption coefficient for shortwave radiation and ε_p is the emissivity of the human body with standard values of 0.7 and 0.97, respectively (VDI 1994, 1998). From R, the T_{mrt} is calculated from Stefan Boltzmann's law (Eq. 2 in L08).

In following, new components of this model are introduced. L08 presents the SOLWEIG model (version 1.0) in detail with an evaluation. Figure 1 provides the structure of SOLWEIG 2.0 with the following improvements that are presented here:

- development and evaluation of a simple vegetation scheme
- inclusion of ground view factors (Ψ_{ground}) for improved estimation of outgoing longwave radiation
- simple approach to estimate nocturnal incoming longwave radiation based on Offerle et al. (2003) for estimating nocturnal T_{mrt}
- modelling of diffuse and direct shortwave radiation
- improved anisotropic estimations of longwave radiative fluxes from the four cardinal points using directional view factors.

Using a spatial domain for the calculations the impact of actual spatial variations in urban geometry can be assessed. To do this, a high-resolution urban digital elevation model (DEM) (Fig. 2a) provides the fundamental site characteristics. SOLWEIG is classified as a 2.5-dimensional model by its use of a 2.5-D DEM (i.e. x and y coordinates with height attributes) to calculate T_{mrt}. The output, in two dimensions (x, y) at a specified height (z=1.1 m) above the surface, has an hourly temporal resolution. The z value is based on the centre of mass of an 'average' person (Fanger 1970). The dimensions of the person can be changed to represent; for example, a male adult or a child depending on the application. In addition, the model can provide the surface radiative fluxes which has applications, for example, in considering architectural shadowing. Other methods and software concerning shadow casting and T_{mrt} modelling are reviewed in L08.

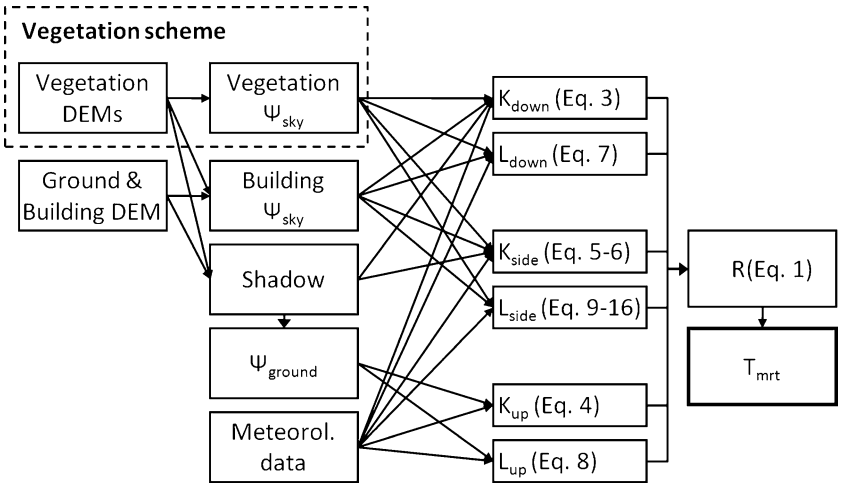

Fig. 1 Flowchart of the SOLWEIG-model where Ψ are images of different view factors. For the equations for each of the radiation fluxes, see text for details

2.1.1 Vegetation scheme

An important influence of vegetation on T_{mrt} comes from shadowing therefore it is critical to have accurate shadow patterns from vegetation within the model domain. The 3-D characteristics of a tree including the presence of a trunk zone (i.e. volume underneath the canopy) (Fig. 2a), the shadow casting procedure in a 2-D grid based environment, which forms the basis of SOLWEIG, is not straight forward. The approach taken here is to introduce two new DEMs to account for the vegetation: (1) for the canopy (Figs. 2b and 3b) and (2) for trunk zone (Figs. 2c and 3c). For the vegetation pixels, the canopy DEM has the height of bushes and/or trees, whereas the trunk zone DEM has the height of the base of the canopy. Thus, each tree has its own shape which is dependent on the spatial resolution of the DEMs.

To cast a shadow the altitude and azimuth of a distant light source (the Sun) are specified. Following Ratti and Richens (1999), 'shadow volumes' are computed by sequentially moving the (e.g. canopy) raster DEM at the azimuth angle of the Sun, reducing the height at each iteration based on the Sun's elevation angle (Fig. 4). At each iteration, a part of the shadow volume is derived and by taking the maximum of this volume for each iteration the whole shadow volume is built up. This is stored as a new DEM. The map of shadows is determined by subtracting the shadow volume image from the original DEM. A Boolean image is produced, with pixels that are ≤0 is in sunlight (new value=1), and positive values is in shade (new value=0). For a detailed description of the shadow casting algorithm, see Ratti and Richens (2004) or Lindberg and Grimmond (2010). When shadow patterns from 3-D objects (e.g. vegetation units) are created, a new more complex shadow casting algorithm is used to generate a separate 'shadow volume' DEM for vegetation units only. In SOLWEIG 2.0, both the canopy and the trunk zone DEM are moving simultaneously based on the position of the Sun. For each iteration, a part of the shadow volume is created only where the pixels in the moving canopy DEM is above the stationary ground and building DEM or stationary canopy DEM at the same time as the moving trunk zone pixels are below (Fig. 4).

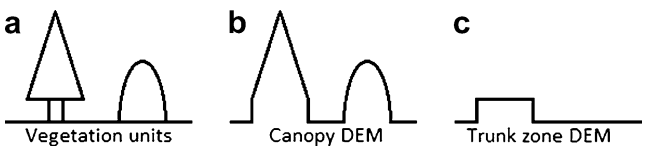

Fig. 2 Cross section of the vegetation representation in SOLWEIG 2. **a** Conifer tree (*left*) and bush (*right*), **b** the canopy DEM and **c** trunk zone DEM based on (**a**)

As shown in Fig. 4, the shadow pattern developed here accounts for the area underneath the vegetation which does not cast a shadow. The importance of the trunk zone varies with the Sun's angle (Fig. 5). At low Sun altitudes, ignoring the trunk zone would introduce a large bias. As the trunk zones areas are used in urban outdoor activities, it is important these are explicitly included in the model. Low Sun altitudes are important at high latitudes in terms of solar access.

The approach taken in SOLWEIG 2.0 is simple but with as accurate estimates of 3-D radiant fluxes and T_{mrt} as possible. To model the 3-D radiant fluxes and T_{mrt}, the following assumptions are made with respect to the vegetation:

- Surface temperature of vegetation is considered equal to air temperature
- Transmission of shortwave radiation through foliated vegetation (τ) is given a constant value of 20% (e.g. Oke 1987; Robitu et al. 2006). However, this value can be altered by the user (see Section 2.2 and 4.2).

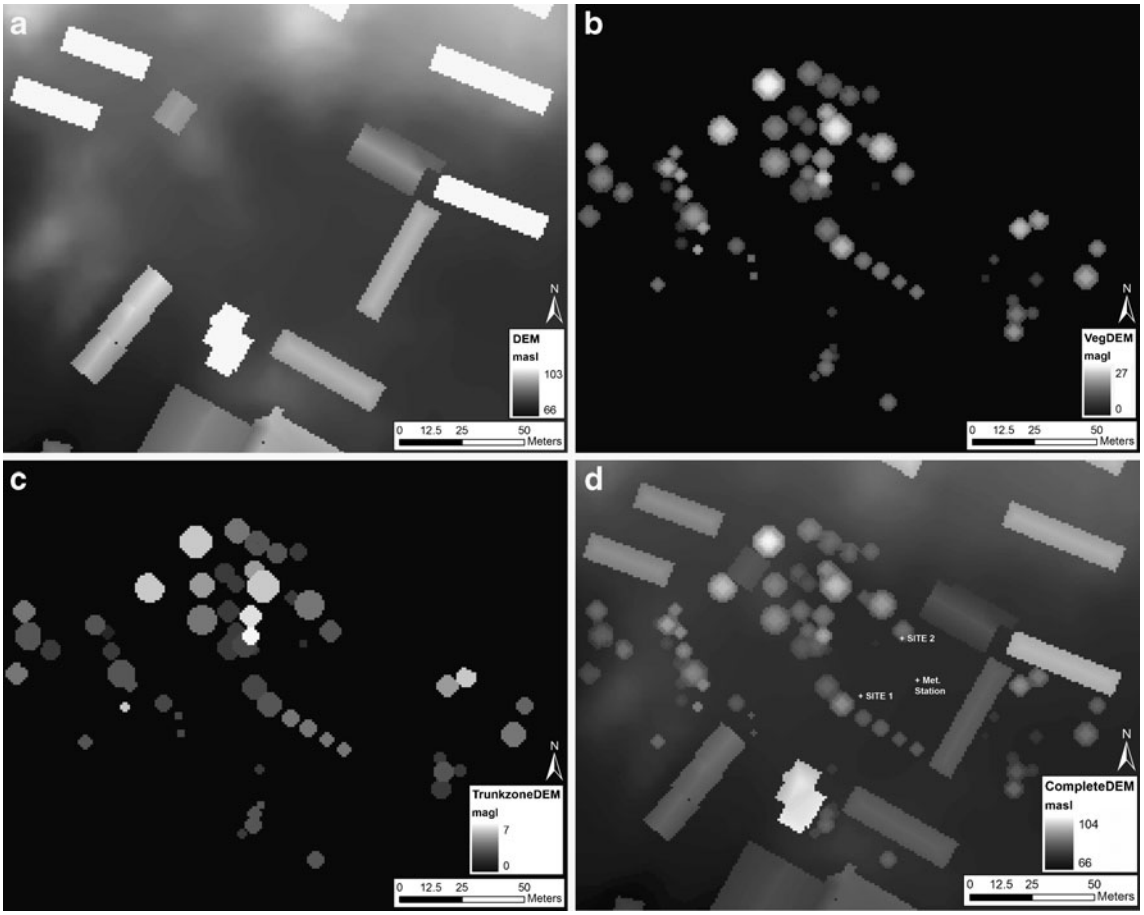

Fig. 3 The GBG2010 study area in Göteborg, Sweden (57°42″ N, 11° 58″ E) and model domain with **a** building and ground, **b** vegetation canopy, **c** trunk zone and **d** complete (building and vegetation) DEMs. Sites 1 and 2 are where integral radiation measurements were conducted. Location of the meteorological station is also given

- Transmission of longwave radiation through foliated vegetation is set to a default value of 0% (Oke 1987)
- Albedo and emissivity of vegetation is treated as constant with values of 15% and 90%, respectively.

2.1.2 Shortwave radiation fluxes

SOLWEIG uses the unobstructed three components of shortwave radiation: direct (I), diffuse (D) and global (G). As these are not commonly available the model also allows calculation of D from G in conjunction with ambient air temperature (T_a) and relative humidity (RH) using the Reindl et al. (1990) approach. Direct shortwave radiation (I) on a surface perpendicular to the Sun is then estimated:

$$I = (G - D)/\sin\eta \tag{2}$$

where η is the Sun's altitude angle above the horizon. Typically within the urban environment, the sky may be obscured by objects (e.g. buildings or trees). Thus, the incoming shortwave radiation ($K_\downarrow$) for a grid cell (x, y) is a function of D, I and G as well as view factors (Ψ). For clarity, the equations are written without the spatial subscript:

$$\begin{aligned} K_\downarrow = {} & I[S_b - (1 - S_v)(1 - \tau)]\sin\eta \\ & + D\left[\psi_{\text{sky } b} - \left(1 - \psi_{\text{sky } v}\right)(1 - \tau)\right] \\ & + G\alpha\left[1 - \left(\psi_{\text{sky } b} - \left(1 - \psi_{\text{sky } v}\right)(1 - \tau)\right)\right] \\ & \times (1 - f_s) \end{aligned} \tag{3}$$

where S accounts for shadow, as indicated in section 2.1 as a Boolean value (presence=0 or absence=1), for buildings (subscript b) and vegetation (v); the subscripts associated with Ψ indicate what aspects are being accounted for (e.g. sky seen by building) and α is the albedo. Currently, α is treated as a constant with a default value of 0.15. τ is the transmissivity of shortwave radiation through vegetation. f_s is the fraction of wall that is shadowed (L08). The first and second terms on the right-hand side of Eq. 3 represent direct and diffuse radiation fluxes, respectively. The third term in Eq. 3 is a simplified representation of reflected radiation.

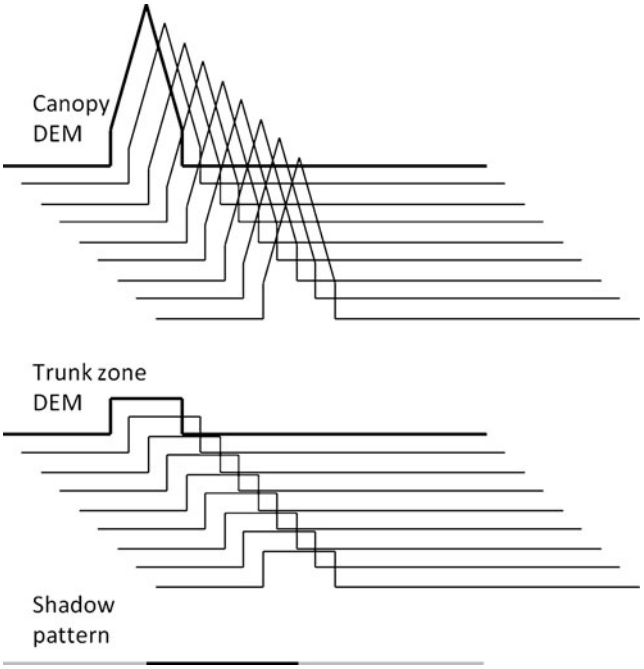

Fig. 4 The repeated translation of a canopy and trunk zone DEM with a simultaneous reduction of their 'heights' which allows detection of shadow patterns from vegetation units such as trees and bushes (below)

The outgoing shortwave radiation ($K_{\uparrow}$) is estimated as:

$$K_{\downarrow} = a\begin{bmatrix} I\left[\psi_{g(\mathrm{sunlit})}(1-\tau)\right]\sin\eta + D\left[\psi_{\mathrm{sky}\,b} - \left(1-\psi_{\mathrm{sky}\,v}\right)(1-\tau)\right] + \\ G\alpha\left[1-\left(\psi_{\mathrm{sky}\,b} - \left(1-\psi_{\mathrm{sky}\,v}\right)(1-\tau)\right)\right](1-f_s) \end{bmatrix} \quad (4)$$

where $\Psi_{g(\mathrm{sunlit})}$ is the view factor of the ground (subscript g) with respect to the amount of sunlit area on the ground seen at z=1.1 m above the ground (centre of mass of a human being). When $\Psi_{g(\mathrm{sunlit})}$=1 only sunlit surfaces are seen from that specific pixel. $\Psi_{g(\mathrm{sunlit})}$ is derived based on the rule-of-thumb resulting from a simple relation that half of the radiative surface influence originates from an area with a radius equal to the sensor height (Schmid et al. 1991). For each pixel a search is conducted at 20° intervals between 0° and 359°. In order not to increase the computational time too much, the maximum search distance is set to 20 times the height of interest (i.e. 21 m when z=1.1 m). Since the shadow patterns are updated every time step (1 h) during the model run, a new image of $\Psi_{g(\mathrm{sunlit})}$ is generated every hour (when η is greater than 0). An example of $\Psi_{g(\mathrm{sunlit})}$, for the same area as Fig. 3d, is shown in Fig. 6. The white linear features visible in Fig. 6 are artefacts of the edge function used to find the location of building walls. For example, if a threshold of 2 m is used then when a change in height of pixels is found the next contiguous pixels must have the same new height for greater than 2 m to be considered a wall. If a building has lower building height somewhere along its perimeter or if a step is present in the DEM, then a certain linear feature is not enclosed and a building footprint is not created.

The shortwave radiation from the four cardinal points ($K_{\rightarrow}$) is based on Eq. 4 and can be estimated as follows (exemplified by the easterly component, subscript E):

If the Sun's azimuth angle (θ) is θ>0° and $\theta\leq$180°

$$\begin{aligned} K_{\rightarrow} = {} & I[S_b - (1-S_v)(1-\tau)]\cos\eta\sin\vartheta \\ & + D\left[1-\left(w_{E\mathrm{wall}} + w_{E\mathrm{veg}}(1-\tau)\right)\right] \\ & + G\alpha\left[w_{E\mathrm{wall}} + w_{E\mathrm{veg}}(1-\tau)\right](1-f_s) \end{aligned} \quad (5)$$

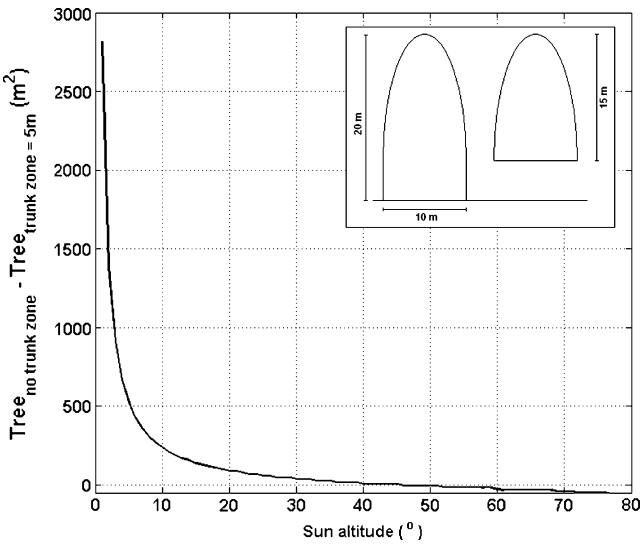

Fig. 5 Difference in shadowed area between a vegetation unit with a trunk zone and without based on Sun's altitude for the two vegetation units with dimensions as shown in inset

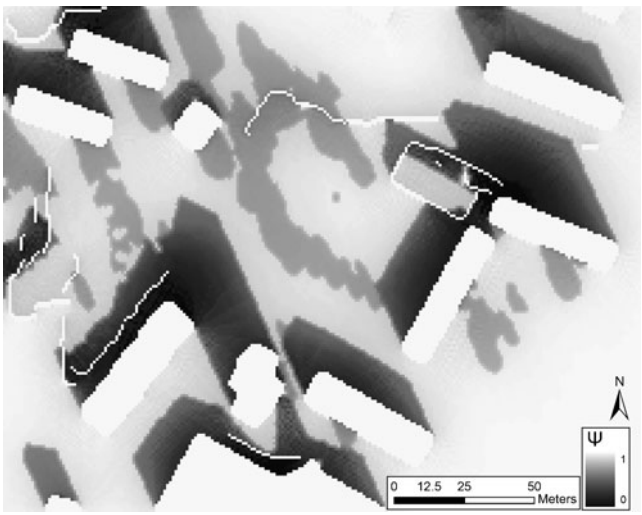

Fig. 6 Ground view factor with respect to amount of sunlit area seen at z=1.1 m above the ground ($\Psi_{g(\mathrm{sunlit})}$) for 11 am on 11 October

else

$$K_{\rightarrow} = D\left[1 - \left(w_{E\text{wall}} + w_{E\text{veg}}(1-\tau)\right)\right] + G\alpha\left[w_{E\text{wall}} + w_{E\text{veg}}(1-\tau)\right](1-f_s) \quad (6)$$

The angular weighting factors (w), explained in detail in L08, represent the amount of radiation originating from either building walls, vegetation, sky as well as all reflecting surfaces seen by a sensor perpendicular to the wall. In SOLWEIG 1.0, it was assumed that the whole hemisphere was included when estimating radiative fluxes from the cardinal points by using Ψ_{sky} when estimating w even though a 'sensor' would only see the eastern part of the hemisphere. Using Lindberg and Grimmond (2010) it is possible to consider view factors from specific cardinal points without creating anisotropic artefacts as occurred formerly when using the Ratti and Richens (1999) method. In SOLWEIG 2.0, directional Ψ are used when deriving w. To calculate shortwave radiation from another cardinal point, e.g. the southerly component, 90° is subtracted from θ in Eq. 5 and the if-condition is changed to if θ>90° and θ≤270°, Eq. 5 else Eq. 6. $w_{E\text{wall}}$ and $w_{E\text{veg}}$ is replaced by $w_{S\text{wall}}$ and $w_{S\text{veg}}$, respectively.

2.1.3 Longwave radiation fluxes

Incoming longwave radiation ($L_{\downarrow}$) is estimated using an equation modified from Jonsson et al. (2006):

$$L_{\downarrow} = \left(\psi_{\text{sky }b} + \psi_{\text{sky }v} - 1\right)\varepsilon_{\text{sky}}\sigma T_a^4 + \left(2 - \psi_{\text{sky }v} - \psi_{\text{sky }vb}\right)\varepsilon_{\text{wall}}\sigma T_a^4 + \left(\psi_{\text{sky }vb} - \psi_{\text{sky }b}\right)\varepsilon_{\text{wall}}\sigma T_s^4 + \left(2 - \psi_{\text{sky }b} - \psi_{\text{sky }v}\right)(1-\varepsilon_{\text{wall}})\varepsilon_{\text{sky}}\sigma T_a^4 \quad (7)$$

where ε_{sky} and $\varepsilon_{\text{wall}}$ are the sky and wall emissivities and T_s is average surface temperature of building walls and ground and T_a is ambient air temperature. All temperatures are in Kelvin. The first term on the right-hand side is the direct sky longwave radiation, the second is the radiation originating from vegetation, the third is the wall radiation and the fourth is the reflected radiation. For a detailed description of the estimation of ε_{sky}, T_s as well as how $L_{\downarrow}$ is modified based on cloud cover, see L08.

Outgoing longwave radiation ($L_{\uparrow}$) is estimated:

$$L_{\uparrow} = \varepsilon_{\text{ground}}\sigma\left(T_s + \psi_{g(\text{sunlit})}(T_s - T_a)\right)^4 \quad (8)$$

The longwave radiation from each of the cardinal points are estimated using the following (exemplified again for the easterly component):

$$L_{\rightarrow E\_\text{SKY}} = \left(\psi_{\text{sky }Eb} + \psi_{\text{sky }Ev} - 1\right)\varepsilon_{\text{sky}}\sigma T_a^4 w_{E\text{sky}} \times 0.5 \quad (9)$$

$$L_{E\_\text{VEGETATION}} = \varepsilon_{\text{wall}}\sigma T_{\text{veg}}^4 w_{E\text{veg}} \times 0.5 \quad (10)$$

$$L_{\rightarrow E\_\text{GROUND}} = L_{\uparrow} \times 0.5 \quad (11)$$

$$L_{\rightarrow E\_\text{REFLECTED}} = \left(L_{\downarrow} + L_{\uparrow}\right)w_{E\text{refl}}(1-\varepsilon_{\text{wall}}) \times 0.5 \quad (12)$$

if θ>0° and θ≤180°

$$L_{\rightarrow E\_\text{SUN}} = \varepsilon_{\text{wall}}\sigma\left(T_a^4 + T_{\text{wall}}^4 \sin\vartheta\right)w_{E\text{wall}}(1-f_{sw}) \times \cos\eta \times 0.5 \quad (13)$$

$$L_{\rightarrow E\_\text{SHADOW}} = \varepsilon_{\text{wall}}\sigma T_a^4 w_{E\text{wall}} f_s \times 0.5 \quad (14)$$

else

$$L_{\rightarrow E\_\text{SUN}} = 0 \quad (15)$$

$$L_{\rightarrow E\_\text{SHADOW}} = \varepsilon_{\text{wall}}\sigma T_a^4 w_{E\text{wall}} \times 0.5 \quad (16)$$

As only half of the hemisphere is taken into account for each cardinal point all terms are multiplied by 0.5.

2.2 The graphical user interface

One objective is to make SOLWEIG easy and assessible to both researchers as well as practitioners, such as urban planners and architects. Hence, the model has a graphical user interface (GUI) with user-friendly windows and buttons rather than command line execution. The GUI, written in Java™, executes the MATLAB Compiler Runtime (MCR). This allows the full functionality of MATLAB without a full version of MATLAB being installed.

The GUI allows the user to change most model input parameters, such as emissivities, albedo, people related parameters used to calculate T_{mrt}, transmissivity of shortwave radiation through vegetation etc. Furthermore, a wizard to create the vegetation DEMs is included as vegetation datasets with 3-D properties are rare. Three types of vegetation are possible in the wizard: coniferous trees, deciduous trees and bushes. Bushes have no trunk zone. The GUI allows calculation of continuous images of

sky view factor DEMs as well as daily shadow patterns from high-resolution urban DEMs. The GUI and the MCR can be downloaded freely from the Göteborg Urban Climate Group-website (http://www.gvc2.gu.se/ngeo/urban/urban.htm).

2.3 Model domain and data

To evaluate SOLWEIG two datasets were collected in Göteborg, Sweden (57°42″ N, 11°58″ E). The study area (termed here, GBG2010) is a square covered with cobble stones and surrounded by two to three storeys buildings except in the north-west where a small park is present (Fig. 2). To the south-west of the square there is a single high rise building (approximately 30 m) and a small pond is located north-west of the square. The vegetation is almost exclusively deciduous trees and bushes. The ground and building DEM, derived from local governmental digital data using the Lindberg (2005) method, has a spatial resolution of 1 m. The canopy vegetation DEM (Fig. 3b) and trunk zone DEM (Fig. 3c) were created using the GUI (Section 2.2). The vegetation location, canopy height, trunk zone height and canopy diameter were obtained from field observations using tape measures and clinometers.

The meteorological forcing data are from a climate station on the roof of Earth Sciences Centre (University of Gothenburg) 100 m south of the square. Air temperature and humidity data were collected using a Rotronic YA-100 and the global and diffuse radiation using a SPN1 Sunshine pyranometer (Delta-T Devices). A second mobile meteorological station recorded T_a, RH, G and wind speed and direction in the centre of the square (Fig. 3d) using the same instruments and mounting as Eliasson et al. (2007). A third station located at two different sites (Fig. 3d) consisted of three net radiometers (Kipp & Zonen, CNR 1) mounted on a steel stand to measure the 3-D radiation fields (Thorsson et al. 2007). The sensors are oriented to measure shortwave and longwave radiation fluxes from the four cardinal points, as well as parallel to the ground surface (incoming and outgoing). The two sites were chosen so vegetation would have large effects on the observed radiative fluxes and T_{mrt}. Site 1 is just north of a row of trees that shadow the area and site 2 is underneath a chestnut tree which receives direct sunlight (Fig. 3d). For model evaluation, data from integral radiation measurements within the model domain were used. In total, measurements were taken over 5 days from early morning to late evening in spring and summer of 2010.

The second dataset, which contains a number of different sites within Göteborg (Sweden), Freiburg and Kassel (Germany), are used to evaluate the model. These data were obtained from joint collaboration with University of Freiburg through the KLIMES-project (Mayer et al. 2008) and University of Kassel. The observations use the same setup as GBG2010 with three net radiometers observing 3-D shortwave and longwave radiation fluxes. These measurements, made at different urban locations where vegetation is absent or sparse, allow evaluation in different urban areas, seasons, weather situations and regional climates.

3 Complete images of sky view factors (Ψ_{sky})

Critical to SOLWEIG calculations is the Ψ_{sky}. The first continuous images of Ψ_{sky} derived from high-resolution urban DEMs were presented by Ratti and Richens (1999). Since then both atmospheric and architectural studies (Ratti and Richens 2004; Ratti et al. 2006; Lindberg 2007; Martilli 2009) have used this raster-based approach to determine spatial variations and characteristics of Ψ_{sky} as well as to derive parameters for urban climate modelling. Chapman (2008) highlighted the issue using the method of deriving continuous Ψ for urban areas since tree coverage, which could be in the range of 20–40% (Oke 1989), is largely ignored.

Using the new shadow casting algorithm (Section 2.1.1) it is now possible to acquire continuous images of the complete Ψ_{sky} with both vegetation and buildings accounted for. It is possible to separate buildings and vegetation to examine the impact of vegetation on Ψ in the urban environment. Figure 7a shows the Ψ_{sky} when only the ground and building DEM are used, whereas Fig. 7b are when only vegetation impacts Ψ_{sky}. It is also possible to consider where vegetation blocks building walls as 'seen' from each pixel within the model domain (Fig. 6c). Directional view factor images similar to the one shown in Fig. 6c are needed to get an accurate weighting factor in Eq. 10. The complete Ψ_{sky}, a combination of Fig. 7a and b is shown in Fig. 7d. In SOLWEIG, Ψ_{sky} is determined prior to calculation of the impact transmission of radiation through the vegetation canopy separately for shortwave and longwave radiation. Visual examination of the different Ψ_{sky} images (Fig. 7) shows the large reduction of Ψ_{sky} underneath vegetation. The view factor values in Fig. 7c are in general high but would probably decrease in a dense urban environment. The mean Ψ_{sky} between Fig. 7a and d is reduced 0.103.

4 Results and discussion

Five days of measurements from GBG2010 and from nine sites in Germany and Sweden are used to evaluate SOLWEIG 2.0. The model is then used to show the spatial and temporal variations of T_{mrt}.

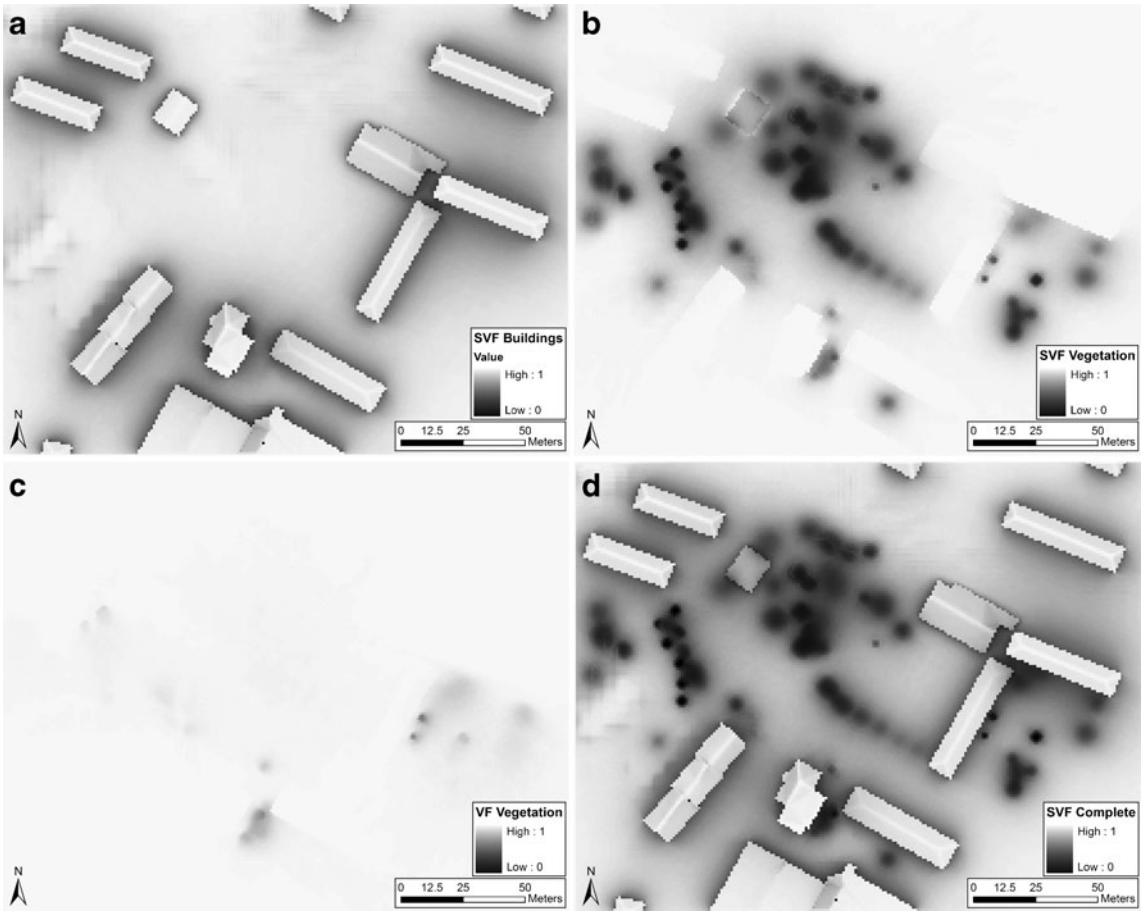

Fig. 7 Continuous Ψ_{sky} for study area GBG2010 using **a** the building and ground DEM, **b** from vegetation blocking the sky, **c** from vegetation blocking the buildings and **d** complete (i.e. both buildings and vegetation)

4.1 Evaluation of building geometry and regional climate on T_{mrt}

Evaluation of SOLWEIG 2.0 covering a range of non-vegetation effects such as building geometry, meteorological variations, regional climates and seasonal aspects are shown in Fig. 8. The evaluation shows almost one to one relations between observed and modelled data. This is an improvement to when SOLWEIG 1.0 was used when a 2°C overestimation of modelled T_{mrt} was evident (not shown). The root mean square error (RMSE) is also reduced from 8.63°C (v1.0) to 6.79°C (v2.0). Scattering increases with temperature (consider 25–55°C; Fig. 8) because the temporal resolution is just one shadow pattern per 1-h period. Thus a pixel is either in the shade or exposed to the Sun for a full hour, which is not always the case. The shadow pattern is generated in the middle of each hour. In reality, a location could be in the shade during the first 40 min of an hour and then exposed to sunlight during the remaining 20 min but SOLWEIG currently assumes that pixel is in the shade for the entire hour. This will result in under- or overestimations of the shortwave radiation fluxes and consequently T_{mrt} in areas that are moving either out of, or into, the shade. Yu et al. (2009) suggest a temporal resolution of 10 min when investigating shadow patterns in complex urban environments. Increasing the temporal resolution increases the computation time considerably but this option will be included in future versions of SOLWEIG.

4.2 Evaluation of vegetation on T_{mrt}

Two different GBG2010 sites were used to evaluate the performance of SOLWEIG with respect to vegetation (Fig. 3d): (1) just north of a row of lime trees (*Tilia cordata*) to examine the impact of vegetation shadowing; and (2) underneath a chestnut tree (*Castanea*) to evaluate T_{mrt} under a vegetation canopy. Four of the five measurement periods were conducted at site 1 and the remaining one at site 2 (Fig. 9). The 5 days were clear to partially cloudy except for May 20th which was cloudy. Site 1 was sunlit until approximately 12 noon LST, and site 2 was sunlit between 12 noon and 4 pm LST. During the remaining period of the measurements both sites were shadowed by vegetation.

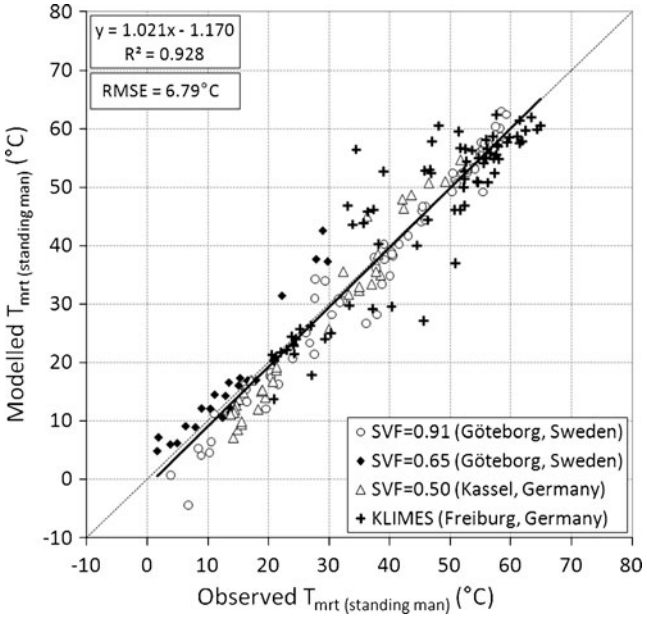

Fig. 8 Observed versus modelled hourly T_{mrt} (n=205). The regression line is based on the combined site data. Data from six different sites with Ψ_{sky} between 0.63 and 0.93 is included from the KLIMES-project

The most evident result seen in Fig. 9 is the considerable improvement of using the vegetation scheme when estimating the radiation fluxes and T_{mrt} at both sites at GBG2010. This is clearest when the two sites are shadowed by the surrounding vegetation canopies. Using the vegetation scheme with a shortwave radiation transmissivity through vegetation (τ) of 20% (open triangles, Fig. 9) results in more realistic model values relative to the observed values compared to not using the vegetation scheme (open squares, Fig. 9). However, modelled T_{mrt} is still overestimated by about 11°C when the vegetation is shading the site. The mean absolute error (MAE) is 5.5°C. This is evident in both the longwave (L) and the shortwave (K) radiation fluxes. This suggests that τ may have been assigned too high a value that will affect K which in turn affects surface temperatures and hence L. Examination of the vegetation canopies through hemispheric photographs (site 1, Fig. 10), suggests τ should be much less than 20%. Reducing τ to 5% (open circles, Fig. 9) reduces the overestimation of T_{mrt} by as much as 6°C and a MAE to 2.74°C. The highest overestimates of T_{mrt}, due to overestimation of the K fluxes, are found during midday (Fig. 9). This is because of the simplification made for reflected shortwave radiation (Eqs. 3–6).

To further examine an appropriate value and to make an improved parameterisation of τ, a comprehensive dataset from Morgan Monroe State Forest (39°19′ N, 86°25′ W), Indiana (Dragoni et al. 2010) were analysed. A full year (2005) of incoming shortwave radiation (15 min averages) from above (46 magl) and beneath a deciduous forest canopy (2 magl) were used to calculate the transmission of global shortwave radiation for different seasons (Table 1). As shown, τ is only 0.07 during the summer months compared to suggested values of 0.2 (Oke 1987; Robitu et al. 2006). The reason for choosing τ=0.05 instead of τ=0.07 is because the competition in a forest reduces the leaf and branch production at lower levels within the forest canopy. Individual trees in urban areas which are separated from each other (Zipperer et al. 1997) are able to develop

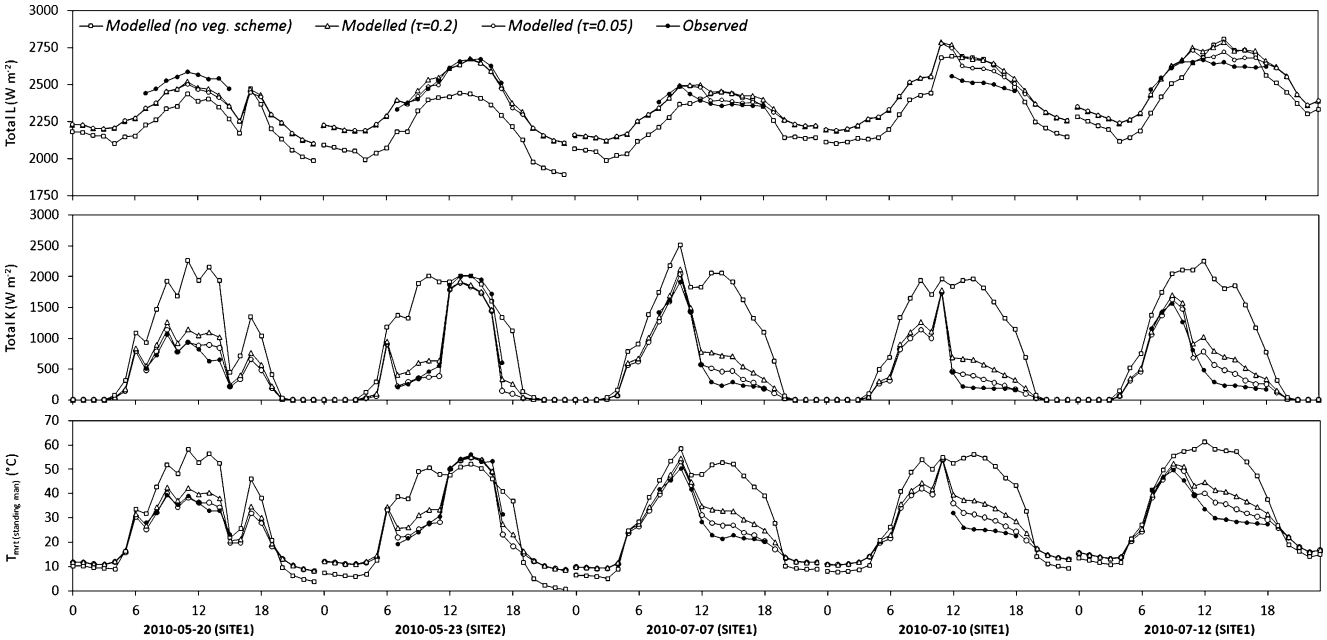

Fig. 9 Observed versus modelled values of total longwave radiation, total shortwave radiation and T_{mrt} at the GBG2010 study area

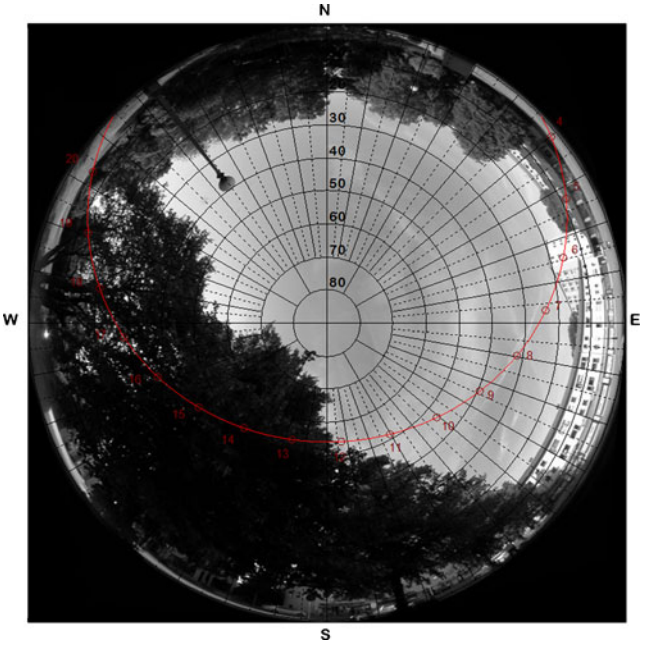

Fig. 10 Hemispheric photograph at SITE 1 (GBG2010). A Sun-path diagram generated for 12th July using ©RayMan Pro (Matzarakis et al. 2009) is included

more branches at all height levels and therefore a slightly lower value of τ could be used compared to a forest area. Results from a sensitivity analysis on how τ affects T_{mrt} in SOLWEIG 2.0, found changing τ from 0.2 to 0.07 reduced the MAE of T_{mrt} from 5.5°C to 3.1°C; and by changing τ to 0.05 reduced the MAE of T_{mrt} an additionally 0.4°C. Hence, a new default value for τ should be 0.05 for fully foliated canopies. The values in Table 1 could be used for other periods of the year.

The assumption that the surface temperature of vegetation is considered equal to air temperature was tested using a handheld IR instrument (AMiR 7811–20) at five different locations within the GBG2010 study area. Observations were made every hour during the 3 days in July while measurements were conducted (n=165). Surface temperature of vegetation followed the ambient air temperature but with a small underestimation of 1.5°C (not shown). A sensitivity test (τ=0.05), with the temperature of vegetation reduced by 1.5°C as shown from the IR temperature measurements, found a very small reduction in T_{mrt} (0.4°C) at the two sites in GBG2010. This implies that the assumption of vegetation temperature being set equal to air temperature is acceptable.

Table 1 Transmission of shortwave radiation (τ) through a deciduous forest canopy (see text for details)

Season	DJF	MAM	JJA	SON
τ	0.43	0.20	0.07	0.20

Figure 11 shows modelled versus observed upward, downward and sideward shortwave and longwave hourly radiation fluxes as well as total fluxes and T_{mrt} from both GCB2010 sites for all 5 days of measurements. As shown, SOLWEIG works well in most situations. However, the overestimation of the shortwave fluxes at lower values (i.e. shadowed by vegetation) creates a larger bias for the smaller T_{mrt}. Nevertheless, SOLWEIG shows an overall good performance of T_{mrt} with a coefficient of determination for the linear regression of 0.91 (RMSE=3.1°C). The highest discrepancies between modelled and observed values are found for the side-facing shortwave radiation fluxes (RMSE=108.1 Wm^{-2}). Shown here are the total fluxes from all four cardinal directions, so therefore the fluxes are smaller when each cardinal direction is considered separately. Overall, the errors are larger for the shortwave fluxes than the longwave fluxes even though the R^2 values are higher for the shortwave fluxes due to the larger span of values (Fig. 11). The total longwave fluxes are larger than the total shortwave fluxes (not shown). Also, one should have in mind the relative greater importance of the longwave fluxes based on the absorption coefficients when estimating R where ε_p is 0.97 and ζ_k is 0.7 (Eq. 1).

4.3 Spatial variations of T_{mrt}

The SOLWEIG model is a non-stationary model that is able to calculate the spatial variation of T_{mrt} at different temporal scales. By using the new vegetation scheme in SOLWEIG 2.0, it is possible to examine how vegetation influences the spatial variation of T_{mrt}. The spatial variation of T_{mrt} in the GBG2010 study area during a clear day in May (3 pm LST, 23 May 2010), when the air temperature was 19.9°C and G was 617 Wm^{-2}, can be seen in Fig. 12. The first obvious features are the shadow patterns, which are essential for the spatial estimation of T_{mrt}: sunlit areas, show considerably higher values of T_{mrt}. The yellow to red areas are exposed to direct sunlight, while the blue areas are in shade from both buildings and vegetation (see online version of Figure). Another clear feature is that T_{mrt} is relatively high close to a building wall (e.g. '**a**' in Fig. 12). An interesting feature is the relatively high values of T_{mrt} for sunlit areas underneath the vegetation canopies (e.g. 'b' in Fig. 12). This is because the vegetation canopies block the relatively colder sky resulting in increased incoming longwave radiation originating from vegetation rather that from sky. Even though T_{mrt} have local maxima at these locations these are probably not areas where enhanced heat stress is believed to occur. By using a thermal index, e.g. physiological equivalent temperature (PET) (Mayer and Höppe 1987)

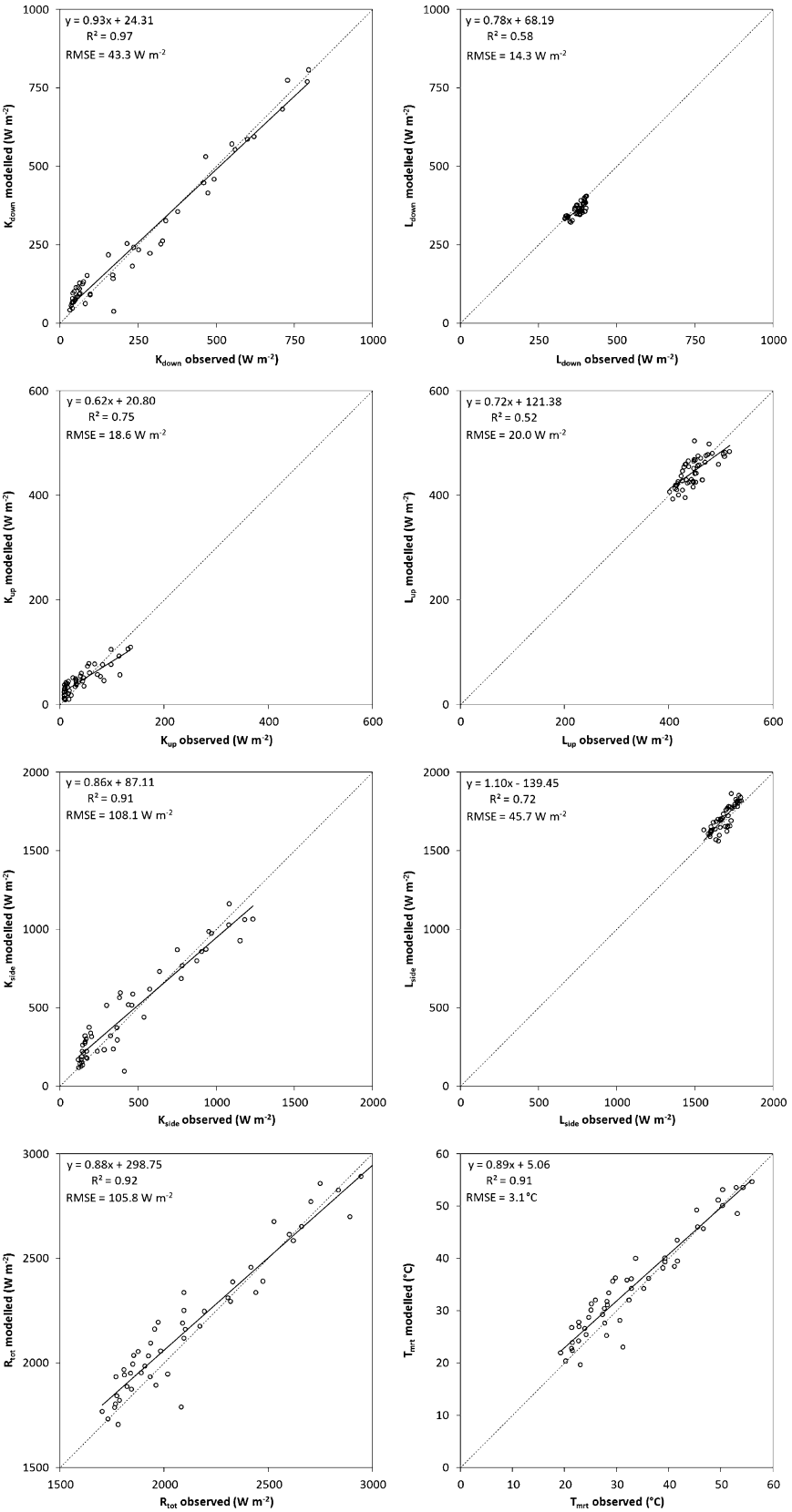

Fig. 11 Observed versus modelled hourly data of the net six directions of shortwave, longwave and total radiation fluxes as well as T_{mrt} at sites 1 and 2 (n=50) within the GBG2010 study area

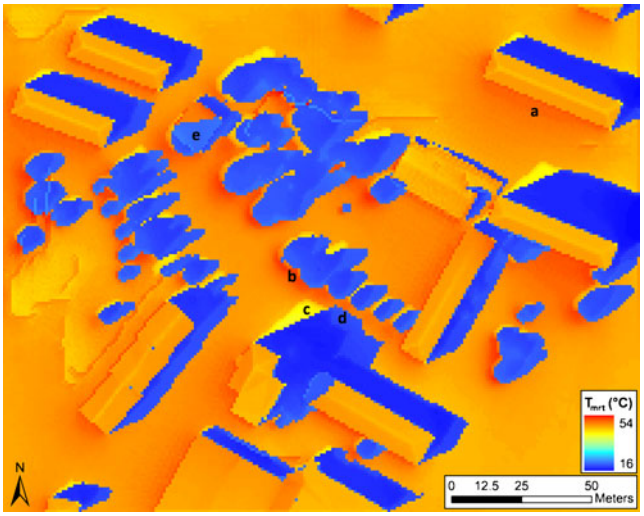

Fig. 12 Spatial variations of $T_{mrt\ (standing\ man)}$ (°C) covering study area GBG2010 at 3 p.m. on 23 May 2010. The spatial resolution is 1 m. The *letters a–e* are points of interest referred to in the text

where the cooling effect by wind is incorporated, areas underneath trees are able to be ventilated to a higher degree compared to areas close to a sunlit building wall (e.g. 'a' in Fig. 12). Also since T_{mrt} is estimated for the centre of gravity of a human, the upper part of a standing body could be in shadow from vegetation while values of T_{mrt} are still estimated as high. Furthermore, episodes of heat stress usually occur in the summer months when Sun's altitude angles are high so the area underneath the vegetation canopy is shaded.

The areas that shift from being exposed to sunlight to becoming shadowed, or reverse, experience a slower rise/drop in T_{mrt} than areas that have been continuously in sunlight or shade for more than 1 h ('c','d' Fig. 12, discussed in greater detail in L08). Vegetation shadowing also occurs on building roofs ('e', Fig. 12) indicating the potential use of SOLWEIG for urban design, e.g. building energy consumption.

5 Future developments

The good performance of the model to date and discussion with potential users has helped to identify where future development efforts to SOLWEIG should be made:

- Currently parameters such as surface albedo and emissivities are spatially constant. In version 3, different properties will be possible through the introduction of a land use grid for each grid cell within the model domain which can have different properties of α, ε, τ etc. This would, e.g. include the possibility to give each vegetation pixel a unique value of τ. Although this will provide a useful tool for investigating the impact of materials, it obviously implies that such detailed data are available so the original default will remain an option.
- Incorporation of PET calculations, which will require spatial variations of wind speeds to be calculated and the use of a database of parameter values for people related to clothing, age, sex etc.
- The temporal resolution will be increased to allow for the suggested 10 min shadow patterns.
- The surface temperature parameterization data are sparse and only available for impervious surfaces. Inclusion of parameterizations of surface material types will be developed.
- The reflection of shortwave radiation should be revisited and improved.

6 Conclusions

A new vegetation scheme for SOLWEIG (version 2.0) is presented which includes a new method to cast shadows from vegetation canopies using a 2.5-D model. The importance of including trunk zone heights (i.e. non-vegetated zones under vegetation canopies) on shadow pattern on the ground is illustrated. Purposely, a very simple approach to the vegetation is taken; specifically, treating the surface temperature of vegetation equal to ambient air temperature, and using the same transmission factors of shortwave and longwave radiation for all trees and bushes.

To evaluate SOLWEIG, a relatively large dataset, given the rarity of such data, is used. The evaluation is done with respect to T_{mrt} at different locations and weather conditions. A high correspondence between observed and modelled values is obtained (R^2=0.93; RMSE=6.79°C; n=205). Modelled values correlate well with observed ones throughout the evaluated temperature range. The scatter increases somewhat between T_{mrt} 25°C to 55°C, due to the current temporal resolution (hourly) of SOLWEIG.

The new vegetation scheme is able to successfully capture the variations of 3-D radiation fluxes and T_{mrt} caused by vegetation (R^2=0.91; RMSE=3.1°C; n=50). A general overestimation is evident when observation points are shadowed by vegetation but the overall error is relatively small (MAE=2.74°C). The assumption that surface temperature of vegetation equals ambient air temperature seems to be fairly reasonable. A mean difference of 1.5°C was found between the two with air temperature lower. A sensitivity analysis showed very small improvement in T_{mrt} when vegetation temperature was increased by 1.5°C.

Given this good performance, future developments are considered worthwhile. A number of suggestions for future development are identified. These would allow the model's continued use for human comfort but also for other applications related to building design, planning and evaluation of instrument exposure.

Acknowledgements This work is financially supported by FORMAS—the Swedish Research Council for Environment, Agricultural Sciences and Spatial Planning and by European Community's Seventh Framework Programme FP/2007–2011 BRIDGE (211345) project. The authors would like to thank the Meteorological Institute, University of Freiburg for providing human-biometeorological data from the KLIMES-project. The interface can be downloaded from the Göteborg Urban Climate Group-website (http://www.gvc2.gu.se/ngeo/urban/urban.htm).

References

Akbari H, Taha H (1992) The impact of trees and white surfaces on residential heating and cooling energy use in four Canadian cities. Energy 17(2):141–149

Akbari H, Kurn DM, Bretz SE, Hanford JW (1997) Peak power and cooling energy savings of shade tree. Energy Build 25:139–148

Akbari H, Pomerantz M, Taha H (2001) Cool surfaces and shade trees to reduce energy use and improve air quality in urban areas. Sol Energy 70:295–310

Ali-Toudert F, Mayer H (2007) Effects of asymmetry, galleries, overhanging façades and vegetation on thermal comfort in urban street canyons. Sol Energy 81:742–754

Ali-Toudert F, Djenane M, Bensalem R, Mayer H (2005) Outdoor thermal comfort in the old desert city of Beni-Isguen, Algeria. Clim Res 28:243–256

ASHRAE (2001) ASHRAE fundamentals handbook 2001 (SI Edition), Vol. American Society of Heating, Refrigerating, and Air-Conditioning Engineers, ISBN: 1883413885

Chapman L (2008) An introduction to 'upside-down' remote sensing. Prog Phys Geogr 32:529–542

Dragoni D, Schmid HP, Wayson CA, Potter H, Grimmond CSB, Randolph JC (2010) Evidence of increased net ecosystem productivity associated with a longer vegetated season in a deciduous forest in south-central Indiana, USA. Glob Chang Biol. doi:10.1111/j.1365-2486.2010.02281.x

Eliasson I, Knez I, Westerberg U, Thorsson S, Lindberg F (2007) Climate and behaviour in a Nordic city. Lanscape Urban Plann 82:72–84

Fanger PO (1970) Thermal comfort. Danish Technical Press, Copenhagen

Gagge AP, Fobelets AP, Berglund LG (1986) A standard predictive index of human response to the thermal environment. ASHRAETrans 92:709–731

Greater London Authority (2010) The draft climate change adaptation strategy for London. pp 138. Available at: http://www.london.gov.uk/climatechange/sites/climatechange/staticdocs/Climiate_change_adaptation.pdf

Honjo T, Takakura T (1990–1991) Simulation of thermal effects of urban green areas on their surrounding areas. Energy Build 15:443–446

Höppe P (1992) A new procedure to determine the mean radiant temperature outdoors. Wetter Leben 44:147–151

IPCC (2007) AR4 Synthesis report, full report, intergovernmental panel on climate change. Available at: http://www.ipcc.ch/pdf/assessment-report/ar4/syr/ar4_syr.pdf

Jonsson P, Eliasson I, Holmer B, Grimmond CSB (2006) Longwave incoming radiation in the Tropics: results from field work in three African cities. Theor Appl Climatol 85:185–201

Lindberg F (2005) Towards the use of local governmental 3-d data within urban climatology studies. Mapp Image Sci 2:32–37

Lindberg F (2007) Modelling the urban climate using a local governmental geo-database. Meteorol Appl 14:263–273

Lindberg F, Grimmond CSB (2010) Continuous sky view factor maps from high resolution urban digital elevation models. Clim Res 42:177–183

Lindberg F, Holmer B, Thorsson S (2008) SOLWEIG 1.0—Modelling spatial variations of 3D radiant fluxes and mean radiant temperature in complex urban settings. Int J Biometeorol 52:697–713

Martilli A (2009) On the derivation of input parameters for urban canopy models from urban morphological datasets. Bound-Lay Meteorol 130:301–306

Matzarakis A, Mayer H, Iziomon MG (1999) Applications of a universal thermal index: physiological equivalent temperature. Int J Biometeorol 43:76–84

Matzarakis A, Rutz F, Mayer H (2009) Modelling radiation fluxes in simple and complex environments: basics of the RayMan model. Int J Biometeorol 54:131–139

Mayer H, Höppe P (1987) Thermal comfort of man in different urban environments. Theor Appl Climatol 38:43–49

Mayer H, Holst J, Dostal P, Imbery F, Schindler D (2008) Human thermal comfort in summer within an urban street canyon in Central Europe. Meteorol Z 17:241–250

Meehl GA, Tebaldi C (2004) More intense, more frequent, and longer lasting heat waves in the 21st century. Science 305:994–997

Offerle B, Grimmond CSB, Oke TR (2003) Parameterization of net all-wave radiation for urban areas. J Appl Meteorol 42:1157–1173

Oke TR (1987) Boundary layer climates. Routledge, Cambridge

Oke TR (1989) The micrometeorology of the urban forest. Philos Trans R Soc Lond B 324:335–349

Pascal M, Laaidi K, Ledrans M, Baffert E, Caserio-Schönemann C, Le Tertre A, Manach J, Medina S, Rudant J, Empereur-Bissonnet P (2006) France's heat health watch warning system. Int J Biometeorol 50:144–153

Picot X (2004) Thermal comfort in urban spaces: impact of vegetation growth—case study: Piazza della Scienza, Milan, Italy. Energy Build 36:329–334

Ratti CF, Richens P (1999) Urban texture analysis with image processing techniques. In: Proceedings of the CAADFutures99, Atalanta, GA

Ratti CF, Richens P (2004) Raster analysis of urban form. Environ Plann B Plann Des 31:297–309

Ratti CF, Di Sabatino S, Britter R (2006) Urban texture analysis with image processing techniques: winds and dispersion. Theor Appl Climatol 84:77–90

Reindl DT, Beckman WA, Duffie JA (1990) Diffuse fraction correlation. Sol Energy 45:1–7

Robitu M, Musy M, Inard C, Groleau D (2006) Modeling the influence of vegetation and water pond on urban microclimate. Sol Energy 80:435–447

Schmid HP, Cleugh HA, Grimmond CSB, Oke TR (1991) Spatial variability of energy fluxes in suburban terrain. Bound-Lay Meteorol 54:249–276

Thorsson S, Lindberg F, Eliasson I, Holmer B (2007) Different methods for estimating the mean radiant temperature in an outdoor urban setting. Int J Climatol 27:1983–1993

Upmanis H, Eliasson I, Lindqvist S (1998) The influence of green areas on nocturnal temperatures in a high latitude city (Goteborg, Sweden). Int J Climatol 18:681–700

VDI (1994) VDI 3789. Part II: Environmental meteorology, interactions between atmosphere and surface; calculation of short-and long wave radiation. VDI/DIN-Handbuch Reinhaltung der Luft, Band 1b, Düsseldorf

VDI (1998) VDI 3789. Part I: Climate. VDI/DIN-Handbuch Reinhaltung der Luft, Band 1b, Düsseldorf

WHO/WMO/UNEP (1996) Climate and health: the potential impacts of climate change. Geneva, Switzerland

Yu B, Liu H, Wu J, Lin W-M (2009) Investigating impacts of urban morphology on spatio-temporal variations of solar radiation with airborne LIDAR data and a solar flux model: a case study of downtown Houston. Int J Remote Sens 30:4359–4385

Zipperer WC, Sisinni SM, Pouyat RV, Foresman TW (1997) Urban tree cover: an ecological perspective. Urban Ecosyst 1:229–246